Molecular Crystals and Liquid Crystals

Publication details, including instructions for authors and subscription information:
http://www.tandfonline.com/loi/gmcl20

Nonlinear Optical Image Processing with Bacteriorhodopsin Polymer Films

Chandra S. Yelleswarapu [a], Pengfei Wu [a], Sri-Rajasekhar Kothapalli [a] & D. V. G. L. N. Rao [a]

[a] Department of Physics, University of Massachusetts, Boston, Massachusetts, USA

Version of record first published: 16 Aug 2006

To cite this article: Chandra S. Yelleswarapu, Pengfei Wu, Sri-Rajasekhar Kothapalli & D. V. G. L. N. Rao (2006): Nonlinear Optical Image Processing with Bacteriorhodopsin Polymer Films, Molecular Crystals and Liquid Crystals, 446:1, 273-294

To link to this article: http://dx.doi.org/10.1080/15421400500379756

Mol. Cryst. Liq. Cryst., Vol. 446, pp. 273–294, 2006

ISSN: 1542-1406 print/1563-5287 online
DOI: 10.1080/15421400500379756

Taylor & Francis
Taylor & Francis Group

Nonlinear Optical Image Processing with Bacteriorhodopsin Polymer Films

Chandra S. Yelleswarapu
Pengfei Wu
Sri-Rajasekhar Kothapalli
D. V. G. L. N. Rao
Department of Physics, University of Massachusetts, Boston, Massachusetts, USA

Real-time medical image processing through nonlinear optical Fourier filtering and transient Fourier holography is demonstrated using bio-organic polymer films of Bacteriorhodopsin (bR). In nonlinear Fourier filtering, the photo-controlled light modulation characteristics of bR films are exploited for early detection of microcalcifications in analog (screen film) as well as digital mammograms. bR films are well known for light modulation between the two states: the initial stable B state with broad absorption band with maximum at 570 nm and the relatively long lived M state with absorption maximum at 412 nm. The spatial frequency information carried by a blue probe beam is selectively manipulated in the bR film by changing the position and intensity of a yellow control beam. In transient Fourier holography, photoisomerizative gratings are recorded and reconstructed in bR films. The laser output from an Ar–Kr ion is expanded and split into two beams. One of them, the object beam is Fourier transformed by a lens on to the bR film placed at the Fourier plane. The second beam (reference beam) overlaps the Fourier transform of the object beam on the bR film thereby recordi00000000ng a Fourier hologram. When the object beam is blocked, the reference beam performs the reconstruction of the recorded Fourier hologram. The filtered spectrum is inverse Fourier transformed on to the CCD camera. The image processing is based on the fact that the desired spatial frequency band is recorded with optimum diffraction efficiency and matching the reference beam intensity to their intensity in the Fourier spectrum. A novel feature of the technique is the ability to transient display selected spatial frequencies in the reconstructing process which enables the radiologist to study the features of interest in time scale. Both the techniques are

This work is supported by National Cancer Institute, NIH grant 1R21CA89673-01A1. The high quality photographic images of the clinical mammograms were obtained from the University of Massachusetts Medical School, Worcester, MA. We thank Dr. Carl D'orsi and Prof. Andrew Karellas for providing them. We also thank Mr. Paul Foster of our Physics Department for providing phantom objects.

Address correspondence to D. V. G. L. N. Rao, Department of Physics, University of Massachusetts, Boston, MA 02125, USA. E-mail: raod@umb.edu

applied to filter out low spatial frequencies corresponding to soft dense breast tissue and display only high spatial frequencies corresponding to microcalcifications in clinical screen film mammograms. The results offer useful information to radiologists for early detection of breast cancer.

Keywords: bacteriorhodopsin film; breast cancer; mammography; optical Fourier processing; spatial filtering

Bacteriorhodopsin (bR) is a photodynamic protein complex found in living systems [1]. It is discovered in 1971 and is related to the visual pigment rhodopsin contained in the cone cells of human retina [2]. The bR rich purple membrane of the *Halobacterium halobium* is responsible for energetic processes in the bacterium [3]. In its natural state the bR molecules perform the biological function in the halobecterial cell of converting light into an electrochemical ion gradient across the membrane. Protons are pumped across the membrane, from the inside (cytoplasmic) to the outside (extracellular) [3]. The pH gradient that results from this proton transfer is responsible for the proton-motive force that allows the bacterium to synthesize ATP from inorganic phosphate and ADP.

The bR molecule contains seven transmembrane helical segments (named A-G) and consists of a polypeptide chain composed of 248 amino acids. The active chromophore in bR protein is a retinal molecule linked via a protonated Schiff base near the middle of helix G to Lysine 216. The relevant location for the proton pumping activity of the bR protein consists of an ion pair which is composed of a protonated Schiff base and an anionic aspartic acid in position 85 (ASP85 residue). Protons transferred from the Schiff base to ASP85 are the primary mechanism in the funneling of protons towards the extracellular side of the membrane and other proton transfers that ensue. This mechanism is also associated with conformational changes of the bR molecule and its chromophoric group during the photocycle [4].

Absorption of a photon by bR triggers the photo cycle which involves a sequence of chemical and physical changes like the retinal molecule's all-trans to 13-cis transformation, shifts of charges within the protein, movement of protons (protonation, deprotonation) and several conformational changes [4,5]. Much of these characteristic changes are reflected in the changes of the bR's absorption spectrum with different states having different lifetimes and characteristic absorption spectra. The quantum yield of the photocycle is relatively high at 64% [6].

Photorefractive materials are widely used for image processing operations such as edge detection, optical correlation etc. [7–9]. But

these materials are expensive and difficult to obtain in large areas. The wonderful thing about bR is ease of preparation as thin polymer films, it has high spatial resolution of over 6000 lines/mm [10], very stable against photo degradation, good low power nonlinear operation, very high quantum efficiency, and environmental friendly. In view of all these advantages bR is widely used for a variety of applications such as optical data storage media, spatial light modulators, photon counters and photovoltaic converters, reversible holographic media, artificial retinas picosecond photodetectors, optical correlators, pattern recognition systems, nonlinear optical filters, spatial filtering, dynamic time-average interferometers, optical limiters, optical logic gates, and optical computing [11–24]. More recently we demonstrated optical image processing using bR films for medical images [25,26].

In this paper we exploited the photo-induced isomerization property of bio-organic polymer films of bR for early breast cancer diagnostics. Breast cancer is one of the leading causes of mortality among women in the world [27]. Early detection of the cancer is extremely important for successful treatment. However, it is not an easy task for the radiologist to quickly and accurately diagnose abnormal pathological changes buried in the soft dense tissue in a mammogram. Among the new sophisticated invasive and noninvasive breast imaging modalities X-ray mammography continues to be the gold standard and is clinically used for detecting the microcalcifications. Several image processing techniques, optical [28–34] and digital [35–39], are available in the literature with main objective of enhancing desired components and filter out undesired components in medical images to aid the radiologist in making a diagnosis and prescribe treatment. Li *et al.* [32] using medical images gave a detail comparison between analog optical and digital image processing techniques. While optical methods enjoy advantages of high speed (due to parallel processing) and high veracity in high frequency regions (using an optimal optical system), the digital methods have the advantages of high processing precision and programmability. Therefore the choice of the method depends on the requirements of clinical setting and the best choice lies in exploring hybrid (analog-digital) techniques that have advantages of high speed, high veracity in high frequencies and programmability.

The spatial filtering, an image processing technique, is ideally suited to enhance the pathological changes in the medical images such as microcalcifications in mammograms. It is well-known from Fourier optics that an optical lens can transform the plane wave into a paraboloidal wave focused at the focal plane of the lens. Different waves with different spatial frequencies are mapped to different points in the focal plane – low spatial frequencies at the center with high

intensity and high spatial frequencies on the edges with low intensity. The low spatial frequencies corresponding to amplitude of the image are physically blocked at the Fourier plane. Inverse Fourier transform of the filtered beam will display only the edges of the image which is the signature of high spatial frequencies. Microcalcifications are tiny calcium deposits in human breast which correspond to high spatial frequencies due to their small size and diffuse nature. Thus the information corresponding to microcalcifications and soft dense tissue background is spatially separated at the focal plane of the Fourier transform and by using spatially filtering technique only the useful information can be displayed [33]. Hence with components like lenses, filters, spatial light modulators (SLM), mirrors and a diode laser, portable systems can be fabricated for medical image processing.

Joseph *et al.* demonstrated experimentally a self-adaptive optical Fourier processing system, using photo-induced dichroic characteristics of bR film with applications in noise reduction, edge enhancement, and bandpass filtering [16]. The filtering technique is based on a mechanism that encodes different spatial frequency components of an input image to different polarization states in bR films using the intensity features of spatial frequency components. The desired components can be selected by an analyzer. This all-optical analog interactive technique is applied for identification of clusters of microcalcifications in mammograms [33]. As the technique does not involve interference of the optical beams, vibration isolation is not required which is a significant advantage over a photorefractive materials in fabricating portable devices.

Here we exploited photo-induced isomerization properties of bR films using the techniques of both photo-controlled light modulation and transient Fourier holography for early detection of microcalcifications in analog (screen film) as well as digital mammograms. In the photo-controlled light modulation technique information carried on one wavelength (blue) is spatially modulated during its passage through the bR film by a second wavelength (yellow) control beam. In the other case transient Fourier holographic gratings are formed by selectively matching the intensities of the desired spatial frequency components in the Fourier spectrum with the reference beam for optimum diffraction efficiency. The techniques are applied to filter out low spatial frequencies corresponding to soft dense breast tissue and display only high spatial frequencies corresponding to the microcalcifications. The results offer useful information to radiologists in breast cancer diagnosis. A significant aspect of the Fourier holographic technique is that the enhanced components in the processed image can be separated in time scale, which further enables the radiologist to monitor these features of interest leisurely by recording and playing the movie.

PHOTO-CONTROLLED LIGHT MODULATION

The photo cycle of bR is shown in Figure 1. In the initial B state of bR, called the light adapted state, the retinal chromophore is in its all-trans molecular configuration. The B state absorbs a yellow photon within the broad bR absorption with a maximum at 570 nm. This-transforms bR into several short lived intermediate states and finally decays to the relatively stable M state (cis) within about 50 μs. The M state can be thermally transformed into the initial B state; the lifetime of this transition depends on the sample preparation. The M state can also be converted into the B state within nanoseconds by absorption of a blue photon corresponding to the peak of M state absorption. For all practical purposes we can neglect the short lived intermediate states of the photocycle. Thus the photo-isomerization of the bR molecules can simply be described as follows:

$$B \underset{R_2,R_T}{\overset{R_1}{\rightleftharpoons}} M$$

where R_i is the rate of the photoisomerization, $i = 1, 2$ corresponding to the photo-isomerizations from B→M (trans to cis) and M→B (cis

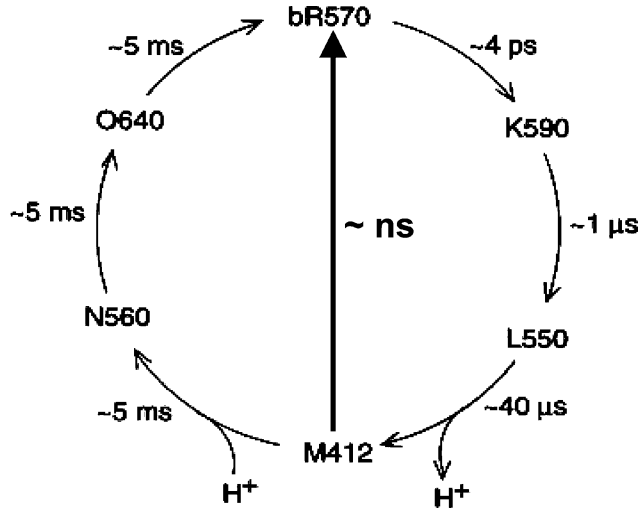

FIGURE 1 bR photocycle. Upon excitation with photon $h\nu_1$ the molecule goes through several short lived intermediate states to the relatively long-lived M state. The molecule goes back to B state via thermal relaxation with lifetime of ~5 ms or a blue photon $h\nu_2$ stimulates the photochemical relaxation to the B state. The numbers next to the alphabets indicate the peak absorption in nanometers.

to trans) respectively while R_T is the rate of the thermal isomerization from M→B. The rate of photoisomerization can be written as [6]

$$R_i = 2302.6\left(\frac{\varepsilon_i \Phi_i \lambda_i}{N_A ch}\right) I_i \tag{1}$$

where ε_i represents the molar absorption coefficient, Φ_i is the quantum efficiency, N_A is the Avogadro's number and h is the Planck's constant. The isomerization rate equation is

$$\frac{dB}{dt} = -R_1 B(t) + R_2 M(t) + R_T M(t) \tag{2}$$

where B(t) and M(t) are the populations of the B and M states. Since a bR molecule can be recycled into a new photocycle after relaxation in to B state, the number of particles in the B⇆M cycle is constant, i.e., $M + B = B_0$, where B_0 represents the total concentration of bR. By a straightforward calculation, we can obtain [40]

$$B(t) = \frac{(R_2 + R_T)B_0}{R_1 + R_2 + R_T}\left\{1 + \frac{R_1}{R_2 + R_T}\exp[-(R_1 + R_2 + R_T)t]\right\} \tag{3}$$

$$M(t) = \frac{R_1 B_0}{R_1 + R_2 + R_T}\left\{1 + \frac{R_1}{R_2 + R_T}\exp[-(R_1 + R_2 + R_T)t]\right\} \tag{4}$$

In the steady state the relative population distribution of B state is obtained by Eq. (3):

$$B_{\text{rel}} = \frac{B(t)}{B_0} = \frac{(R_2 + R_T)}{R_1 + R_2 + R_T} \tag{5}$$

This equation is valid for optical thin films where the light intensities are considered to be constant throughout the volume. Since the B and M states are both photoactive and their absorption bands partially overlap, each wavelength λ_i in principle induces both trans → cis and cis → trans reactions. Hence the absorption of light of the ith wavelength λ_i in the bR film of thickness dz, which is dependent on its own intensity and the other intensity I_j is described by the Beer-Lambert law. The absorption $\alpha(\lambda_i, I_j)$ of a light of wavelength λ_i with intensity I_j is superimposition of the absorption coefficients $\varepsilon_B(\lambda_i), \varepsilon_M(\lambda_i)$ and the populations of B (I_j) and M (I_j) states

$$\alpha(\lambda_i, I_j) = \{\varepsilon_M(\lambda_i) + [\varepsilon_B(\lambda_i) - \varepsilon_M(\lambda_i)]B_{\text{rel}}(I_j)\}B_0 \tag{6}$$

For numerical approximation, the bR film of thickness d is treated as a stack of N slices with each having thickness of $\Delta z = d/N$. Then the

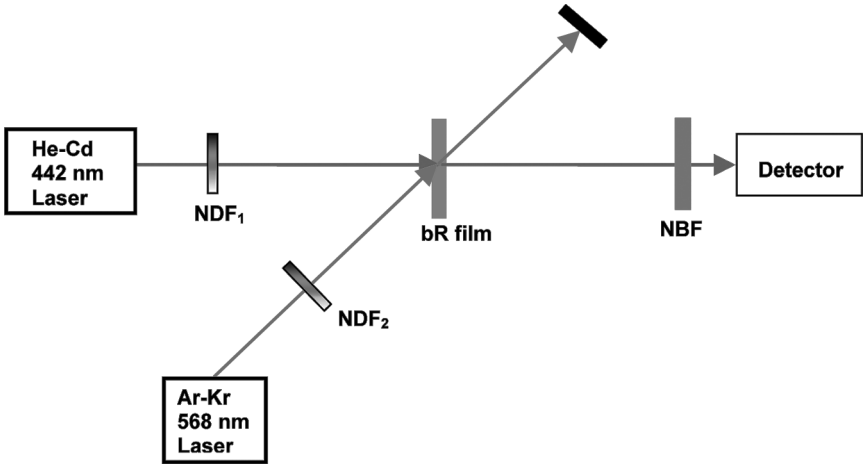

FIGURE 2 Schematic of the experimental setup to study the photo-controlled light modulation characteristics of bR film. NBF: narrow band filter to block the stray yellow light; NDF: neutral density filters.

intensities transmitted through the bR film can be recursively calculated from the following equation with n running from 0 to $N-1$ and $I_{i,N} = I_{i,T}$;

$$I_{i,n+1} = I_{i,n} \exp\left[-2.3026\alpha(\lambda_I, I_j)\Delta z\right] \tag{7}$$

which gives the intensity dependent transmission as $T_i(I_j) = I_{iT}/I_{i0}$. By simulating the above Eqs. (6) and (7) for the intensity dependent transmission, Thoma *et al.* [6] showed that the local transmittance of a bR film depends on the ratio between the forward (B→M) and the backward (M→B) photoreactions. Thus bR films can be used as light controlled absorptive spatial light modulators with applications in spatial filtering. The transmittance for a yellow information-carrying wave of 568 nm can be increased with red light (B→M), e.g., 633 nm, or can be decreased with blue light (M→B), e.g., 413 nm.

Similarly when the information is carried on a blue beam the transmittance can be controlled with a yellow beam. A simple experiment is performed, as shown in Figure 2, to demonstrate intensity dependent transmission characteristics of a bR film at 442 nm (probe beam) with 568 nm control beam and vice versa. The wild-type bR film used for the study is purchased from Munich Innovative Biomaterials GmbH and has optical density of about 5 at 570 nm with thickness of $\sim 100\,\mu$m. Transmittance of the probe beam is measured at the output at detector

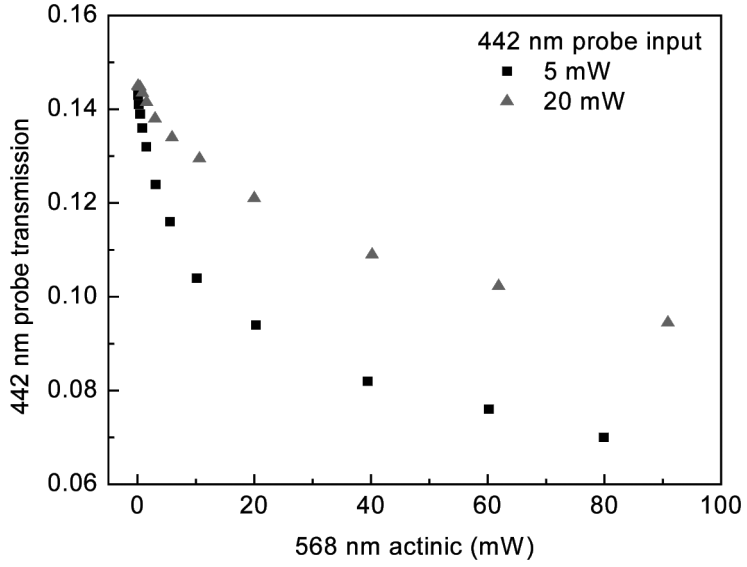

FIGURE 3 Transmission characteristics of 442 nm probe beam as a function of 568 nm control beam intensity. Probe transmission decreases due to the availability of more bR molecules in M state caused by B→M photo-isomerization process as the control beam intensity is increased.

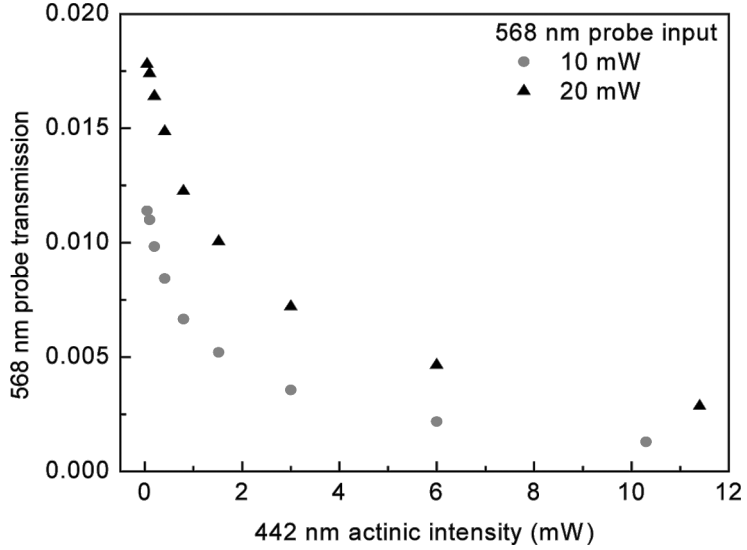

FIGURE 4 Transmission of 568 nm probe as a function of intensity of 442 nm control beam.

plane by varying its input intensity using a neutral density filter. The intensity of control beam is kept constant throughout the measurement. The experiment is repeated for various control beam intensities. The input power is measured using a Melles Griot broadband power meter model #13PEM001, while the output is measured using Newport power/energy meter model #1825 C. The results displayed in Figure 3 show the transmission of bR film at 442 nm decreases with increase in 568 nm control beam intensity. Similarly the results displayed in Figure 4 show that the transmission of the film at 568 nm probe beam decreases with increase in 442 nm control beam intensity. These results in agreement with the simulations of Thoma *et al.* [6].

Processing of Phantoms and Screen-Film Mammograms

Results shown in Figures 3 and 4 demonstrate an important feature that the probe transmission of one wavelength can be significantly reduced by the control beam of a different wavelength in the high intensity region. Based on these results we designed a simple experimental scheme for the real-time image processing of phantoms as well as real clinical mammograms as shown in Figure 5. The probe beam 442 nm from a He–Cd laser and control beam 568 nm from an Ar–Kr laser are both spatially filtered and well collimated. The 442 nm beam illuminates the object, either the phantom or the clinical mammogram. A 10.5 cm focal length convex lens (L_1) is used to obtain the Fourier spectrum. The bR film is placed at the Fourier plane and the inverse Fourier transform is obtained with another 10.5 cm focal length lens (L_2). The processed images are captured on the CCD and displayed on the monitor. Now the yellow control beam is tightly focused on to the bR film spatially overlapping the blue beam for real-time image processing. Initially when there is no control beam then the entire information of the object carried by the blue light is passed through bR virtually without any processing. When the control beam is turned on, some B molecules are excited to M state only in the overlapped region which results in decrease in the transmission of the information carrying blue beam. As the overlapped region contains only low spatial frequencies they are selectively absorbed leaving the high spatial frequencies intact. Therefore the transmitted pattern of the blue light captured by the CCD contains predominantly high spatial frequencies only corresponding to microcalcifications. The low spatial frequencies corresponding to dense soft background tissue are filtered out.

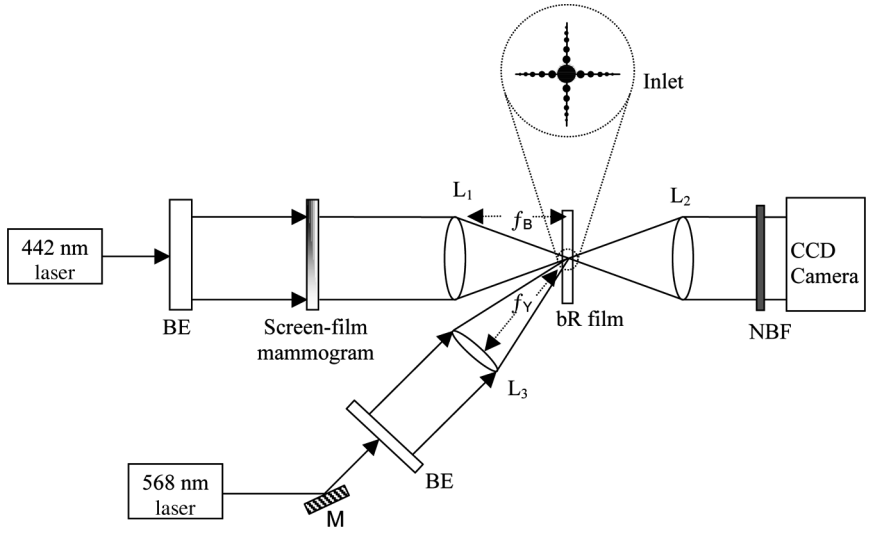

FIGURE 5 Experimental setup for processing clinical screen-film mammograms using photo-controlled light modulation characteristics of bR film. L: converging lens, f: focal length, NBF: narrow band filter to block 568 nm at CCD plane; NDF: neutral density filter; BE: beam expander; M: mirror. Inlet: Schematic showing the patial overlap of two beams at the bR film plane (which is normal to the optic axis of the blue laser beam).

The feasibility of the technique is established initially with different shapes and sizes of phantom objects as shown in Figure 6(a), (c) and (e). Different shapes of objects give rise to different types of spatial frequency spectra at the Fourier plane where bR is placed and it demonstrates that the technique works for processing any complex frequency spectrum. For Figure 6(a), the high spatial frequency spectrum at Fourier plane has only vertical and horizontal directions where as for Figure 6(c) it is distributed in the circular manner. Similarly the image in Figure 6(e) has arc shape edge in addition to horizontal and vertical edges, therefore its high spatial frequency components at the Fourier plane are distributed in circular, vertical and horizontal directions. The processed images of Figure 6(a), (c), and (e) are shown in Figure 6(b), (d) and (f) respectively clearly displaying the edge enhanced versions of the original image. The results demonstrate the enhancement of high spatial frequency components for different shapes and sizes of object.

In the traditional masking technique when the object is changed the filter has to be changed and aligned precisely for blocking the low

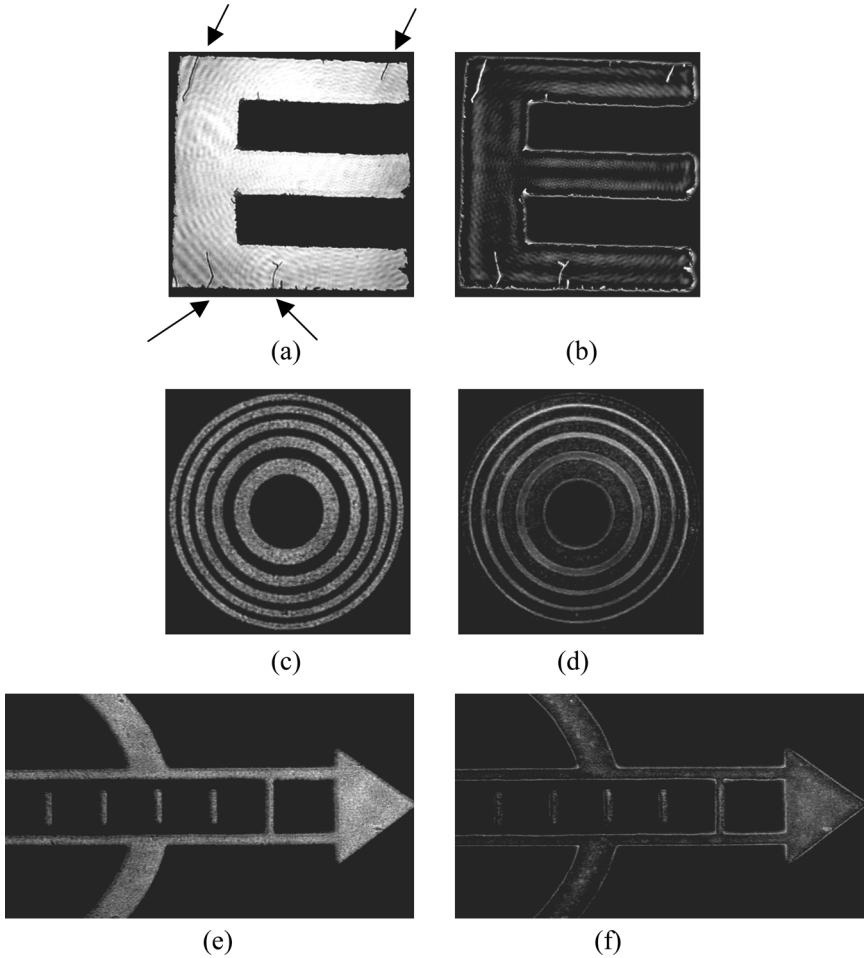

FIGURE 6 (a) , (c) & (e) represent original images of "E," concentric bright circle and an arrow captured by CCD camera in absence of yellow light in Figure 4; (b), (d) & (f)'s represent respective processed images captured by CCD camera in the presence of yellow light.

spatial frequencies. The advantage of this technique is it involves a less cumbersome operation of moving the lens or controlling the yellow beam intensity to achieve the low spatial frequency filtering because center of the low spatial frequencies remains at the same focal spot though their spatial extent changes. We replaced the phantom objects by analog screen film mammograms. Figure 7(a) and (d) display original screen film mammograms used in the experiment. Figure 7(b) and

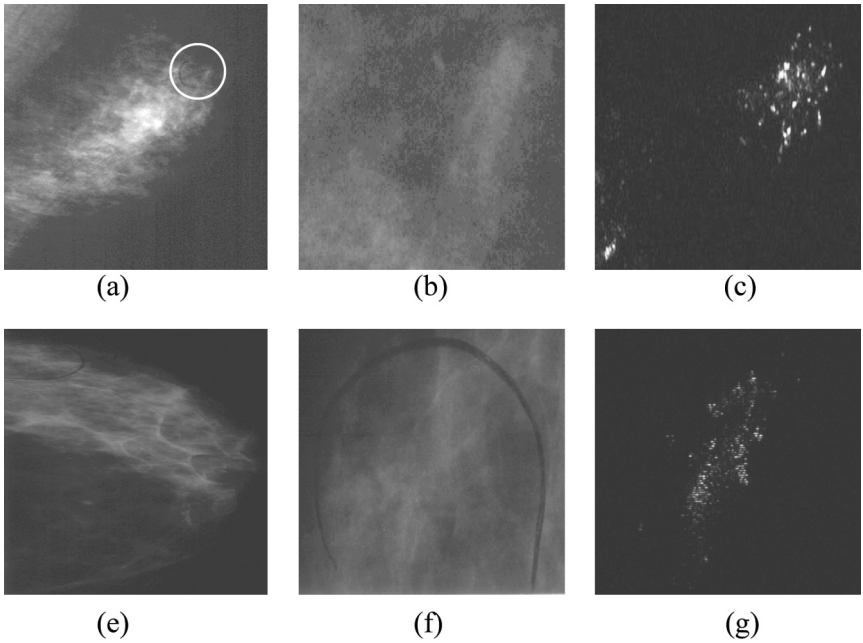

FIGURE 7 (a) Scanned version of film mammogram used in the experiment shown in Figure 4 with ROI encircled; (b)'s magnified ROI; (c)'s processed image of ROI in film mammogram.

(e) display the respective scanned versions of region of interest (ROI). The ROI's in the original Film mammogram are illuminated by blue light as shown in the experimental setup Figure 3. As discussed previously, the yellow control beam induces photo-controlled isomerization in bR film and thus reducing the transmission of low spatial frequency components. The background of soft dense breast tissue corresponding to low spatial frequencies in the Fourier spectrum is filtered out at the bR plane. On the other hand, the high spatial frequencies corresponding to microcalcifications are transmitted. Figure 7(c) and (f) show the reconstructed image displaying only microcalcifications which are not visible to the naked eye in the original clinical mammogram.

Processing of Digital Phantoms and Digital Mammograms

As digital mammography is becoming popular in recent years in view of advantages of digital techniques, we illustrate the application of our

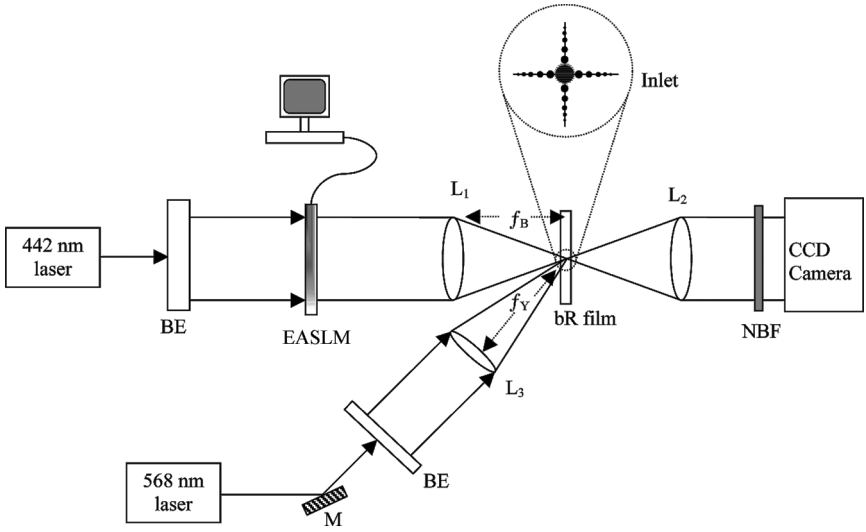

FIGURE 8 Experimental setup for processing digital phantoms and clinical digital mammograms using photo-controlled light modulation characteristics of bR film L: converging lens, f: focal length, NBF: narrow band filter to block 568 nm at CCD plane; NDF: neutral density filter; BE: beam expander; M: mirror. Electrically addressed spatial light modulator (ESLM) facilitates the interface between digitally stored mammogram in the computer and the optics used in the experiment. Collimated laser beam through ESLM bears the information of the object that is displayed on the SLM.

technique also to digital phantoms and mammograms. An electrically addressed spatial light modulator (SLM) is incorporated into the experiment, as shown in Figure 8, to facilitate the interface between digitally stored mammogram in the computer and the optics used in the experiment. The collimated He–Cd 442 nm laser beam illuminates the SLM and the output of the SLM is a coherent optical signal bearing the image displayed on the SLM. The resulting optical image is then processed as discussed above. Initially we studied digital phantoms shown in Figure 9(a) and (c). Thus the reconstructed image captured by the CCD camera as shown in the Figure 9(b) is edge enhanced. Similarly Figure 9(c) shows a digital phantom containing white simulated microcalcifications buried in gray background. Contrast between white pixels used to simulate microcalcifications and surrounding grey pixels used to simulate background of soft dense breast tissue is so small, that the microcalcifications are not visible to the naked eye. Figure 9(d) shows the reconstructed image

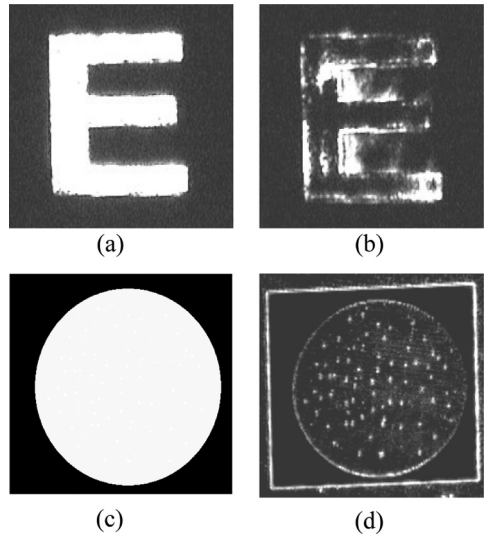

FIGURE 9 (a) and (c) are original images of "E" and phantom with simulated microcalcifications – white spots buried in white back ground with little gray level difference; (b) and (d) are corresponding processed images reconstructed with high spatial frequencies.

displaying only high spatial frequencies corresponding to the simulated microcalcifications now visible to the naked eye. Figure 10 shows the results for clinical digital mammograms. Figure 10(a) is the original digital mammogram (with ROI encircled with black ink) displayed on the SLM from the computer monitor. Figure 10(b) shows the digitally magnified ROI and Figure 10(c) shows the reconstructed image

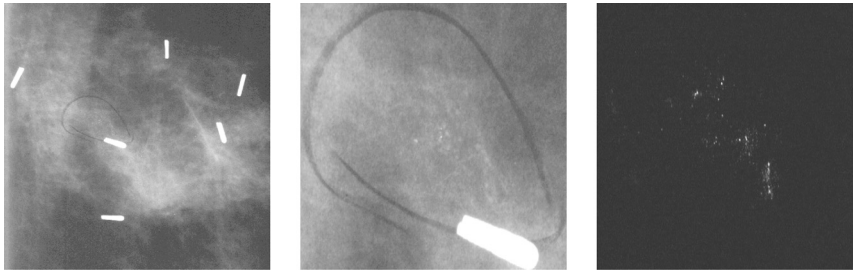

FIGURE 10 (a) Digital film mammogram used in the experiment with ROI encircled; (b) magnified ROI; (c) processed image of ROI of (a).

with high spatial frequencies captured by CCD clearly showing the microcalcifications with good contrast.

TRANSIENT FOURIER HOLOGRAPHY

We also exploited the temporal and intensity dependent features of diffraction efficiency of Fourier holograms recorded in bR molecules for transient nonlinear spatial filtering and applications to medical image processing. Hologram is recorded in the bR film by interference of two coherent beams at suitable angle obtained from the same laser. Due to the spatial intensity modulation induced by the interference of the two recording beams in the sample, the photoisomerization from B→M is spatially modulated leading to a M state population grating. The modulated contrast of the M state population grating is described by [40]

$$\Delta M(t) = \left(\frac{\partial M(t)}{\partial I_2}\right)\Delta I \tag{8}$$

where ΔI is the modulated contrast in the interference field of the light. The diffraction efficiency of this grating is proportional to the square of modulated contrast ΔM(t). From Eqs. (3) and (4), the temporal behavior of the modulated contrast in the reading process is given as

$$\Delta N_2(t) = \frac{(A_1A_2)IB_0}{(1+(A_1+A_2)I)^2}\exp[-(1+A_2I)R_Tt] \tag{9}$$

where $A_iI = R_i/R_T$. From the Eq. (9) it follows that the dependence of the grating contrast decreases as the reading beam intensity increases resulting in decay of the diffracted signal. This is confirmed by performing a simple experiment with the schematic shown in Figure 11. The 568 nm output from an Ar–Kr ion laser (Coherent Innova 70 C Spectrum) is expanded by a beam expander to a diameter ~2.5 mm, and then split into two beams by a 50–50 beam splitter. These two beams are recombined over a small angle (~10°) in the bR film. The object beam power is varied using variable neutral density filter, while the reference beam power is kept constant. The intensity of the reference beam is fixed at 26 mW/cm^2 while intensity of the object beam is varied from 1.6 mW/cm^2 to 1.6 W/cm^2, to simulate the range of intensities of spatial frequencies in the Fourier spectrum of the object. The holographic grating formed due to the interference between the two beams is recorded in bR film for about

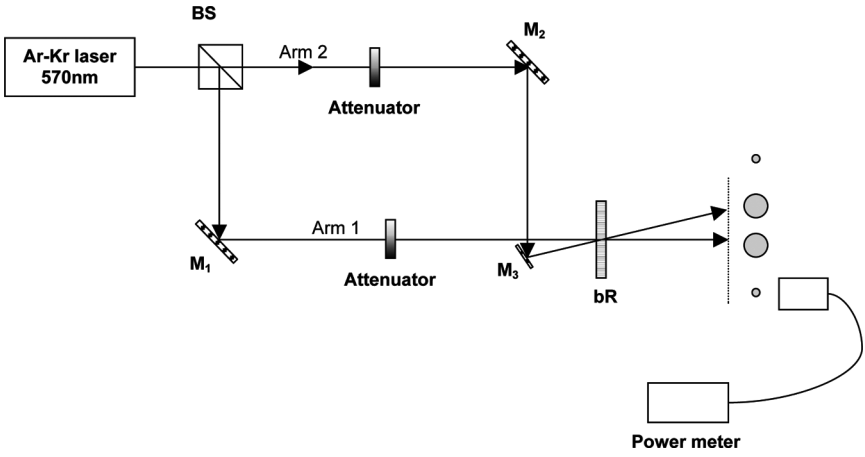

FIGURE 11 Schematic of the experimental setup used to study temporal and intensity dependent properties of hologram grating recorded in bR film. M: mirrors; BS: beam splitters; and L: lenses.

5 sec to reach its saturation. The optimum of diffraction efficiency occurs when object beam intensity is matched to the reference beam intensity. The object beam is blocked and the reference beam reconstructs the object information. The intensity of the diffraction signal as read by the reference beam is measured. When the object beam is blocked and the reading beam is on, the grating contrast decreases due to isomerization process from M→B resulting in decay of the diffracted signal. Figure 12 shows the decay of diffraction signal with time for an object beam intensity of 26 mW/cm^2 and matched reference beam intensity of same value. We observed decay of the diffraction signal for a series of object beam intensities. The values of diffraction signals obtained from this data are plotted as a function of object beam intensities for various time delays shown in Figure 10 inlet. It is clear that the diffraction efficiencies show optimum values when the object beam intensity matches the reference beam. At either low or high intensity region of the object beam, the diffraction efficiency decreases. Theoretical fit (solid line in Fig. 12) using Eq. (9) to the experimental curves is good for both the grating contrast and decay time dependence on reference beam intensity. In addition, our experimental results of the diffraction decay can be explained in terms of two lifetimes. For good theoretical fitting to the experimental curves, in Eq. (9) we used two exponential decay times corresponding to two lifetimes, 62 ms and 240 ms. We believe the short one originates

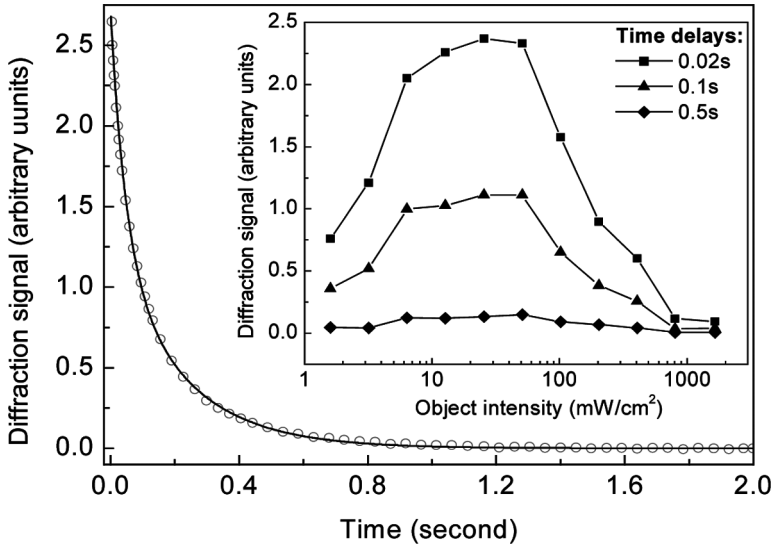

FIGURE 12 Temporal decay of diffraction signal when object and reference beam intensities are matched at 26 mW/cm^2. Solid line is the theoretical fit and open circles are experimental results. Inlet: Diffraction signal as a function of object beam intensity for various time delays. Reference beam intensity is fixed at 26 mW/cm^2.

from the isomerization rate M→B, and the long one is due to the mechanism of bR molecular reorientation. Diffraction decay data for other object intensities can also be explained similarly.

We exploited the temporal and intensity dependent features of diffraction efficiency of bR molecules by recording of selected spatial frequencies for applications in image processing. To illustrate the feasibility of the technique we first recorded the high spatial frequencies of a binary test object using the experimental setup shown in Figure 13. The laser output from 568 nm output from an Ar–Kr ion laser is expanded using beam expander and then split into two beams. One of the beams, object beam, is passed through an object E and is transformed to Fourier plane by a lens with focal length of 20 cm. The other, reference beam, spatially overlaps the Fourier transformed object beam on the bR film at the Fourier plane thereby recording the Fourier hologram. A variable attenuator in the reference path is used to match its intensity to that of the desired spatial frequency band in Fourier spectrum of the object beam for maximum diffraction efficiency. After recording the hologram, about 5 seconds, the object

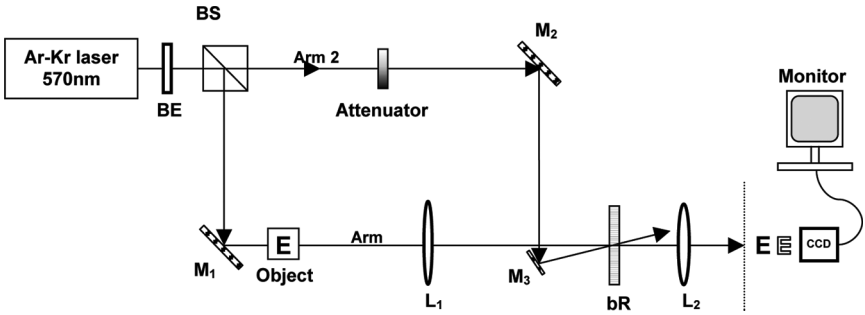

FIGURE 13 Experimental setup for study of enhancement of spatial frequencies of an object using transient Fourier holography. M: mirrors; BE: beam expander; BS: beam splitters; and L: lenses.

beam is blocked and the reference beam performs the reconstruction of the recorded Fourier hologram. The desired frequency band is inverse Fourier transformed and is imaged on to the CCD camera. The reconstructed wave shows an edge enhancement effect as shown in Figure 14. As bR material also has saturable absorption feature, it offers the advantage of directly transmitting low-frequency components of the image as they correspond to high intensity in the Fourier spectrum. We do not require the reference beam. This is illustrated in Figure 14(c) with the soft edge of object E corresponding to low spatial frequencies. Thus this scheme can give processed results of both low-frequency and high-frequency components in real time and can in principle be adopted for other frequency bands also.

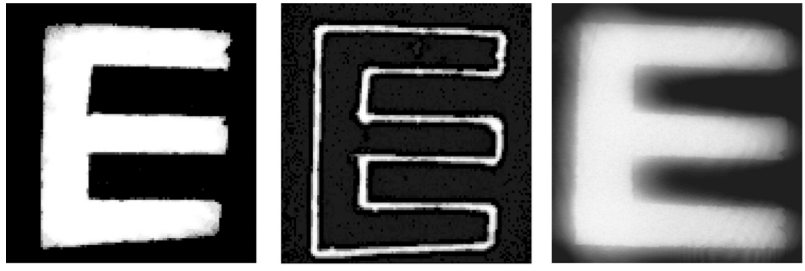

FIGURE 14 Experimental results of Image processing using Fourier holography. For the binary image "E": (a) original, (b) edge-enhanced, and (c) edge-softened.

We then applied this scheme for processing clinical mammograms for early detection of microcalcifications. The object E in the above experiment is replaced with region of interest (ROI marked by the radiologist) of the mammogram. By controlling the reference intensity, edge enhancement of mammograms is achieved leading to clear display of microcalcifications (not visible in the original mammogram to the naked eye of the radiologist) on the monitor. We present results for two such mammograms in Figure 15. An additional attractive feature of this technique is the transient nature in display of different spatial frequencies in the Fourier spectrum of an object. Since different spatial frequencies correspond to different intensities, from the Figure 12 inlet we can infer that at a given time, all the spatial frequencies exist though at different diffraction efficiencies, the optimum efficiency occurring for selected band of frequencies which match the reference beam intensity. Thus we can distinguish between different spatial frequencies as they reveal at different times. To demonstrate this concept we used a resolution chart (USAF negative target,

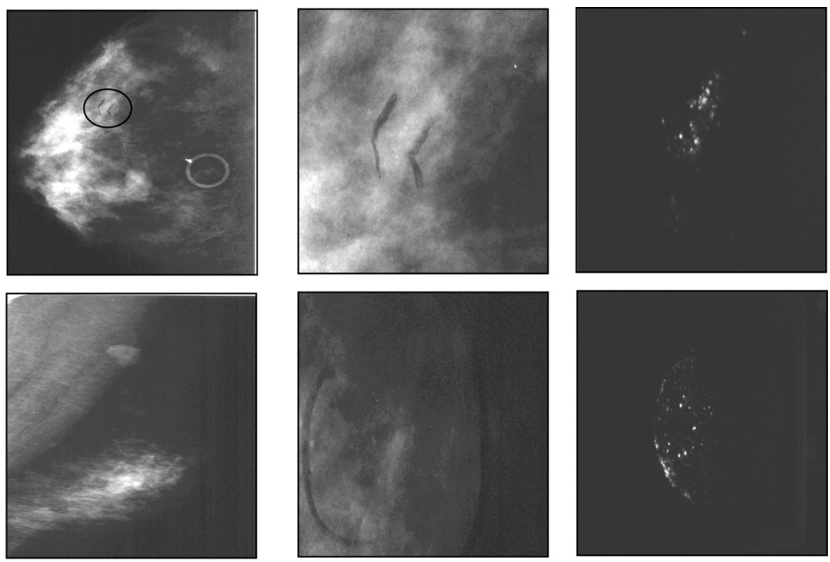

FIGURE 15 Experimental results of image processing using Fourier holography. For the mammograms: (a) originals with region of interest (ROI) circled by radiologists, (b) blow-up of the ROI; (c) processed images showing calcifications.

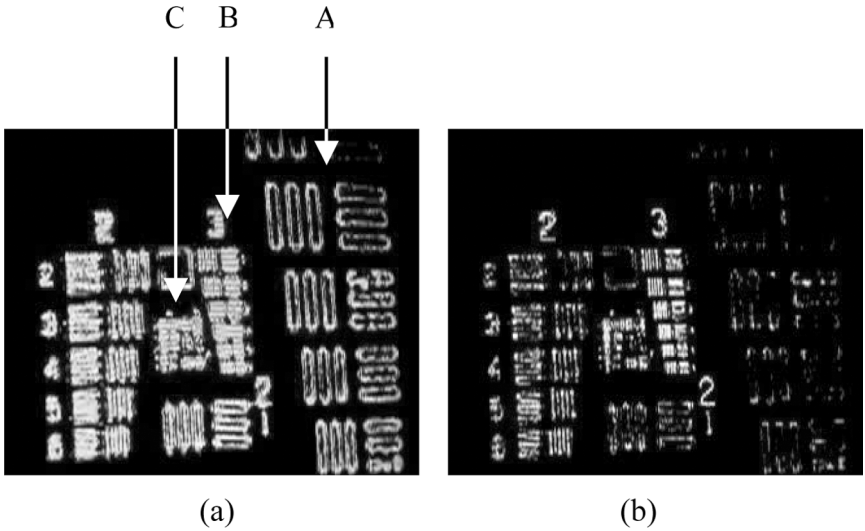

FIGURE 16 Transient display of spatial frequency information of grating resolution chart captured at times (a) t = 0; and (b) t = 5 seconds.

Edmund Optics). As shown in Figure 16 at time t = 0 we can observe all the frequency groups (A – low frequency group, B – middle frequency group and C – high frequency group) but at a later time at t = 5 sec only the frequency group B which matches the reference beam intensity remains clear while other frequency groups vanish. This could be a potential advantage to the radiologist in diagnostics as the various features in the mammogram occur at different scales – such as clusters of micro-calcifications at small scales, edges of smooth or star-shaped objects at middle case and architectural distortions at large scales. A recorded movie can be viewed a leisure by the radiologist to look at all the features that are revealed in time scale.

CONCLUSION

In conclusion, interesting results on temporal and intensity-dependent properties of Fourier holographic gratings using bR films are reported. The analysis using a theoretical model based on photoinduced isomerization agrees with our experimental results. We exploit this technique to process mammograms in real-time for detection of micro calcifications buried in the background of soft tissue and noise. The results are useful to radiologists for diagnostics of breast cancer. In addition, we found that the information in static processed images

can be further separated in time scales. These temporal image features offer useful information to the radiologist about the pathological changes in the image which cannot be obtained from the static processed image. Finally, digital mammograms are expected to replace their conventional analog counterparts because of sophisticated storage and processing technology. But due to large volume of data, it is difficult to create scalable systems for the prompt storage, retrieval and processing of mammograms. With the advent of optical storage technologies using Fourier holography, the optical technique proposed in this paper can easily be adopted for integrated processing and storing the data.

We studied light modulation characteristics of bR films using two wavelengths. The results of intensity dependent transmission demonstrated that the relative population of bR molecules in B and M states can be controlled using two different wavelengths. The spatial frequency information carried by a probe beam is selectively manipulated in bR film by changing the position and intensity of the control beam. Feasibility of the technique is established by processing different shapes and sizes of phantom objects that have complex spatial frequency distribution at the Fourier plane. The technique is applied to filter out low spatial frequencies corresponding to the soft dense tissue displaying only microcalcifications corresponding to high spatial frequencies in clinical screen film mammograms. Since digital mammography is now becoming popular, we adapted the system using an electrically-addressed SLM for processing digital phantoms and mammograms. The technique is hybrid in nature and can offer high speed as well as programmability advantages needed for an ideal clinical setting. As there is no need of vibration isolation in the experiment, it is possible to build a portable device. The technique has potential for optical implementation of wavelet transform and image subtraction that could be exploited for medical image processing application.

REFERENCES

[1] Sharkov, A. V. & Matveets, Y. A. (1987). *Laser Picosecond Spectroscopy and Photochemistry of Biomolecules*. V. S. Letokhov (Ed.), Adam Hilger: Bristol, U.K., 56.
[2] Andrews, D. L. (1990). *Lasers in Chemistry*, Springer-Verlag: Berlin.
[3] Birge, R. R. & Zhang, C. F. (1990). *J. Chem. Phys.*, *92*, 7178.
[4] Oesterhelt, D., Bräuchle, C., & Hampp, N. (1991). *Q. Rev. Biophys.*, *24*, 425.
[5] Dér, A., Oroszi, L., Kulcsár, Á., Zimányi, L., Tóth-Boconádi, R., Keszthelyi, L., Stoeckenius, W., & Ormos, P. (1999). *Proc. Natl. Acad. Sci. USA*, *96*, 2776.
[6] Thoma, R., Hampp, N., Brauchle, C., & Oesterhelt, D. (1991). *Opt. Lett.*, *16*, 651.
[7] Jack Feinberg. (1980). *Opt. Lett.*, *5*, 330.
[8] Chang, T. Y., Hong, J. H., & Yeh, P. (1990). *Opt. Lett.*, *5*, 743.

[9] Banerjee, P. P., Gad, E., Hudson, T., McMillen, D., Adbeldayem, H., Frazier, D., & Matsuhita, K. (2000). *Appl. Opt.*, *39*, 5337.
[10] Yuan, Z., Bao-Li, Y., Ying-Li, W., Neimule, M., Ming, L., Guo-Fu, C., & Hampp, N. (2003). *Chinese Phys. Lett.*, *20*, 671.
[11] Rao, D. V. G. L. N., Aranda, F. J., Narayana Rao, D., Chen, Z., Akkara, J. A., & Nakashima, M. (1996). *Opt. Commun.*, *127*, 193.
[12] Downie, J. D. (1994). *Appl. Opt.*, *33*, 4353.
[13] Nikolai Vsevolodov. (1998). *Biomolecular Electronics: An Introduction via Photosensitive Proteins*, Birkhauser: Boston.
[14] Birge, R. R., Gillespie, M. B., Izaguirre, E. W., Kuznetzow, A., Lawrence, A. F., Singh, D., Wang Song, Q., Schmidt, E., Stuart, J. A., Seetharaman, S., & Wise, K. J. (1999). *J. Phys. Chem. B*, *103*, 10746.
[15] Imam, H., Lindvold, L. R., & Ramanujam, P. S. (1995). *Opt. Lett.*, *20*, 225–227.
[16] Joseph, J., Aranda, F. J., Rao, D. V. G. L. N., Akkara, J. A., & Nakashima, M. (1996). *Opt. Lett.*, *21*, 1499.
[17] Huang, T. & Wagner, K. H. (1993). *Appl. Opt.*, *32*, 1888.
[18] Sánchez-de-la-Llave, J. D. & Fiddy, M. A. (1999). *Appl. Opt.*, *38*, 815.
[19] Miyasaka, T. (1995). *Jpn. J. Appl. Phys.*, *34*, 3920.
[20] Okamoto, T., Yamagata, K., & Yamaguchi, I. (1997). *Jpn. J. Appl. Phys.*, *36*, 1012.
[21] Mikaelian, A. L. (1996). Holographic memory and some applications. In: *Optical Storage and Retrieval*, Yu, F. T. S. & Yutamulia, S. (Eds.), 31–74.
[22] Sánchez-de-la-Llave, J. D. & Pommet, D. A. (1998). *Opt. Engg.*, *37*, 27.
[23] Berg, R. R. (March 1995). *Protein-Based Computers*, Scientific American, 90.
[24] Lewis, A., Albeck, Y., Lange, Z., Benchowski, J., & Weizman, G. (1997). *Science*, *275*, 1462.
[25] Kothapalli, S. R., Wu, P., Yelleswarapu, C. S., & Rao, D. V. G. L. N. (2004). *Appl. Opt.*, *85*, 5836.
[26] Kothapalli, S. R., Wu, P., Yelleswarapu, C. S., & Rao, D. V. G. L. N. (2005). *Journal of Biomedical Optics*, 10, 0440281.
[27] American Cancer Society, *Breast cancer facts & figures 2003–2004*, [Online] Available: http://www.cancer.org/downloads/STT/CAFF2003BrFPWSecured.pdf
[28] Goodman, J. W. (1991). *Opt. Photon, News*, *2*, 11.
[29] Heanue, J. F., Bashaw, M. C, & Hesselink, L. (1994). *Science*, *265*, 749.
[30] Javidi, B. & Horner, J. L. (1994). *Real-Time Optical Information Processing*, Academic Press: Boston, MA.
[31] Goodman, J. W. (1968). *Introduction to Fourier Optics*, McGraw-Hill, Inc: New York, 141–197.
[32] Yuhua Li, Wei R. Chen, Yimo Zhang, Wei Qian, & Hong Liu. (2002). *J. Biomed. Opt.*, *7*, 255.
[33] Wu, P. & Rao, D. V. G. L. N. *Proceedings SBMO/IEEE MTT-S IMOC*, 689, (2003).
[34] Panchangam, A., Sastry, K. V. L. N., Rao, D. V. G. L. N., DeCristofano, B. S., Kimball, B. R., & Nakashima, M. (2001). *Med. Phys.*, *28*, 22.
[35] Pal, S. & King, R. (1981). *Electronic Letters*, *17*, 302.
[36] Morrow, W., Paranjape, R., Rangayyan, R., *et al.* (1992). *IEEE Trans. Med. Imaging*, *11*, 392.
[37] Laine, A. F., Schuler, S., Fan, J., *et al.* (1994). *IEEE Trans. Med. Imaging*, *13*, 725.
[38] Wang, T. C. & Karayiannis, B. N. (1998). *IEEE Trans. Med. Imaging*, *17*, 498.
[39] Kothapalli, S. R., Yelleswarapu, C. S., Naraharisetty, S. R. G., Wu, P., & Rao, D. V. G. L. N. (2005). *Academic Radiology.*, 12, 708.
[40] Wu, P., Wang, L., Xu, J., Zou, B., Gong, X., Zhang, G., Tang, G., & Chen, W. (1998). *Phy. Rev. B*, *57*, 3874.